Deep-Sea Research II 129 (2016) 394–400

Contents lists available at ScienceDirect

Deep-Sea Research II

journal homepage: www.elsevier.com/locate/dsr2

Lagrangian predictability in the DWH region from HF radar observations and model output

Max Yaremchuk*, Peter Spence, Mozheng Wei, Gregg Jacobs

Naval Research Laboratory, Stennis Space Center, MS 39529, United States

ARTICLE INFO

Available online 2 June 2013

Keywords:
Variational interpolation
High-frequency radars
Lagrangian trajectories

ABSTRACT

Predictability of surface drifter trajectories in the Deep Water Horizon oil spill region is used as a criterion for optimizing the parameters of the 2d variational (2dVar) interpolation of high-frequency radar (HFR) data, and assessing the accuracy of the surface currents' simulations by regional models. It is shown that penalizing the magnitude and enforcing smoothness of the divergence field significantly increases the Lagrangian predictability of the 2dVar output at the forecast times of 3–9 days while preserving it at the shorter forecast times. Applying preliminary gap-filling technique based on the analysis of spatial correlations of the radial velocities adds an extra 1–2% to the 2dVar forecast skill. Comparison of the forecast skills provided by the 2dVar interpolation of the HFR data and the assimilative solutions of the Navy Coastal Ocean Model demonstrates 25–30% better skill of the 2dVar product, indicating potential benefits of assimilating HFR data into regional models.

Published by Elsevier Ltd.

1. Introduction

In recent years considerable efforts have been made to study predictability of the trajectories of the floating material at the sea surface (Özgökmen et al., 2001; van Sebille et al., 2009; Lumpkin and Elipot, 2010; Huntley et al., 2011). This problem is important in many applications, including search and rescue missions, accident localization via backward tracking of the debris, or optimization of the protective missions in response to environmental disasters.

Since numerical modeling became the major forecast tool in oceanography a large literature appeared on the Lagrangian predictability (LP) of the velocity fields produced by the models. The major parameter, characterizing the LP of a model is the root-mean-square (rms) separation e_τ between the observed and model-simulated drifters for a given forecast time τ. A few years ago Barron et al. (2007) conducted a comprehensive LP study of the Navy Layered Ocean Model by comparing drifter tracks in 30 regions of the World Ocean with the trajectories simulated by the model. The estimated values of e_τ varied in the range between $e_1 \approx$10–25 km for $\tau = 1$ day and increased to 50–150 km for $\tau = 7$ days. Later, Huntley et al. (2011) studied the LP of the Navy Coastal Ocean Model (NCOM) at 1/16° resolution in the South China Sea documenting the values of $e_1 = 17$ km and $e_7 = 145$ km. They also observed that coarsening of spatial resolution up to 1/2° had a relatively small impact on the LP. In contrast, reduction of the temporal resolution to 12–20 h significantly reduced the LP due to poor resolution of tidal currents. In the most recent study, Scott et al. (2012) have shown that LP of the model output could be improved by taking the ensemble average of the drifter trajectories produced by several models. In particular, the value of e_1 was reduced from 27 km to 21 km when averaging over five models of the equatorial Atlantic was performed.

In general, it appears that a typical model value of e_1 varies within 15–25 km and rarely falls below 10 km (in the latter case, as a rule, the background flow is strong and exhibits small shear). It is also noteworthy that LP is weakly affected by data assimilation (Scott et al., 2012), unless independent velocity observations are taken along the drifter trajectories.

In this respect, development of the coastal HFR networks (Harlan et al., 2010) can be considered as a major observational support for increasing the accuracy of the Lagrangian forecasts in the near-shore regions. HFR observations are capable of delivering information on surface currents that is consistent in both space (1–5 km) and time (0.2–1 h) resolutions of the regional circulation models. Therefore, in recent years a lot of studies have been devoted to LP comparisons of the surface currents derived from HFR observations by various techniques. As a few examples, Ullman et al. (2006) investigated the skill of the HFR-derived currents in predicting drifter trajectories on the Atlantic coast of the US and obtained the value of $e_1 \approx$5–7 km, using Lagrangian tracking with a random flight model to simulate the effect sub-grid turbulence on the trajectories; Kohut et al. (2012) employed 8 drifters to assess the parameters of the optimal interpolation scheme which was used to obtain gridded velocities from the HFR

* Corresponding author.
E-mail address: max.yaremchuk@nrlssc.navy.mil (M. Yaremchuk).

0967-0645/$ - see front matter Published by Elsevier Ltd.
http://dx.doi.org/10.1016/j.dsr2.2013.05.035

observations off the New Jersey coast, obtaining the value of e_1≈8 km; Shadden et al. (2009) have shown a substantial coherence between the drifter trajectories and the HFR-derived Lyapunov exponents in the Monterrey Bay. In their recent work, Barrick et al. (2012) demonstrate a good forecast skill of a simple statistical model of the surface currents derived from HFR data by the OMA technique (Kaplan and Lekien, 2007).

These results indicate that HFR observations have a better forecasting capability on their own right, and may substantially increase the LP of the surface velocity fields after being assimilated into the numerical models.

In the present study we assess LP of the HFR-derived currents during the Deep Water Horizon (DWH) oil spill (May–December 2010). In particular, we explore the impacts on the LP of the preliminary gap-filling and of suppressing divergence of the HFR currents obtained by the 2d variational algorithm (Yaremchuk and Sentchev, 2009, 2011). The LP is used as a benchmark in estimating the overall accuracy of HFR observations in the DWH region and optimization/tuning the 2dVar interpolation scheme. The potential benefit of assimilating HFR data into regional models is assessed by comparing the LPs of the HFR-derived velocity fields with the data-assimilative NCOM output.

The paper is organized as follows. In the next section, we delineate the study area, and describe the data. In Section 3, the methodologies used to estimate surface currents and the respective Lagrangian trajectories are outlined. Then in Section 4 we compare the trajectory forecast skill statistics for various HFR interpolation products and for the assimilative NCOM model runs. We conclude with a summary of the key results and their implications for further studies of the DWH region.

2. Observations in May–December 2010

2.1. HFR observations

Radial sea surface currents were measured by three CODAR SeaSonde systems operating along the northern Gulf of Mexico (NGOM) coast in the region east of the Mississippi mouth. The three-site long-range (~4.5 MHz) system provided hourly surface currents at 6 km radial and 5° azimuthal resolution over the region shown in Fig. 1. Radial velocities observed at each of the 3 sites were obtained with the MUSIC algorithm (Schmidt, 1986) using measured antenna patterns. These data were obtained from NOAA National Data Buoy Center HFR archive.

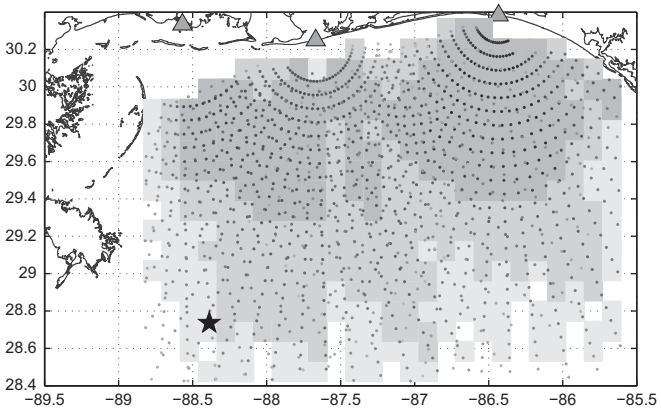

Fig. 1. HFR coverage of the DWH region. Dots show locations of the radial velocity observations from the three radars denoted by gray triangles. Intensity of the gray color of a dot is proportional to the total observation time during the period between 7 May and 31 December, 2010. Shaded areas delineate subdomains covered by HFR observations more than 80% of time (dark gray), 65—80% of time (gray) and 50—65% of time (light gray). The DWH location is shown by the black star.

The acquired radial velocity data were characterized by inhomogeneous coverage both in space and time (Fig. 2). The temporal patchiness was caused by multiple reasons, mostly by malfunctions of the radars (e.g., in the beginning of August) and required filling the gaps in the space-time coverage of the domain by observations prior to retrieving the gridded velocity fields from the data. The utilized gap-filling method (Yaremchuk and Sentchev, 2011) is similar to the technique used in preprocessing satellite SST data that are often obscured by clouds. After filling of the gaps, hourly velocity vector fields were reconstructed using the variational interpolation method described in the next section.

The effective depth of the measured surface currents depends on the HFR frequency. Under the assumption of a linear surface current vertical profile the effective measurement depth is proportional to the radar wavelength with the proportionality coefficient of $1/8\pi$ (Stewart and Joy, 1974). Therefore, the effective depth of the current measurements is estimated to be ~2.6 m.

Assessment of the uncertainties provided by the CODAR systems was made under the assumption that the respective errors σ- are $\delta-$correlated in space. The error estimates were made using statistical analysis of the radial velocities in the course of the gap-filling. The resulting values of σ were computed as square roots of the azimuthally averaged diagonal elements of the noise covariance matrix and varied from 4 cm/s to 16 cm/s for the ranges between 15 and 240 km. These numbers are consistent with the typical error estimates of the long-range CODAR systems. The values of σ were used in the definition of the cost function weights in the 2dVar algorithm for retrieving the vector fields from the observed radial components.

2.2. Drifter trajectories

We used the observed trajectories of satellite-tracked drifters available at the Naval Oceanographic Office database for the 8 months (May–December) of 2010. The database contains drifter data from many sources including the AOML Drifter Data Assembly Center (www.aoml.noaa.gov/phod/dac/dacdata.html and the US Coast Guard. In addition we used quality controlled drifter trajectories from the Ocean Circulation Group at the University of South Florida. These data included drifters that were deployed in the eastern Gulf of Mexico region in summer 2010 as a rapid response to the Deepwater Horizon oil spill (Liu et al., 2011; Weisberg, 2011).

Most of the drifters were drouged to follow currents near the 1–2 m depth, which is consistent with the effective depth range of the currents registered by the HFRs. The drifters have been tracked with several satellites, with 1 h time between the fixes. We used the quality-controlled drifters interpolated to 1-hourly positions in the time interval between May 7, and December 31 of 2010. In space, the domain was limited to the area of HFR coverage (Fig. 1). All the drifter tracks considered were located within the regular 6 km grid (Fig. 3) used for HFR data interpolation (see Section 3.1). Drifter trajectories observed between May 7 and December 31, 2010 in the study area are plotted in Fig. 3.

On the total, 37 drifters (comprising 297 drifter-days) were used in the analysis. It should be noted that the major part of the trajectories are located in the regions with relatively poor HFR coverage (cf. Figs. 1 and 3): many drifters were released immediately after the spill in the vicinity of the DWH site (Fig. 3), which was covered by coastal radars only 55% of the time (Fig. 1). Temporal coverage was also uneven: 75% of the data (226 drifter-days) were acquired in the period between May 7 and July 31, 2010.

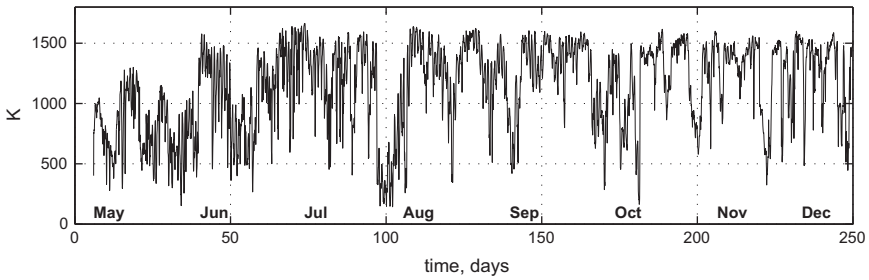

Fig. 2. The total number K of the radial velocities measured by three HF radars as a function of time.

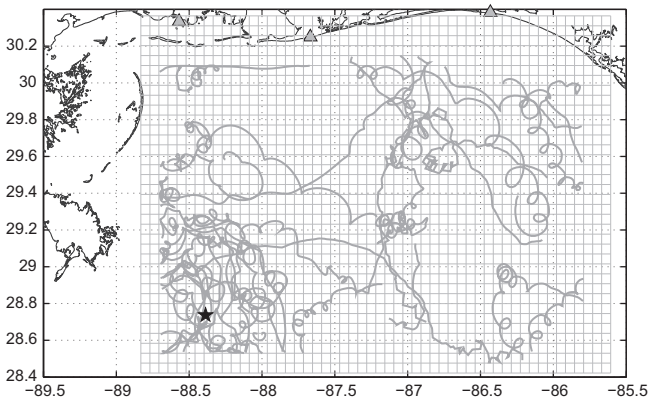

Fig. 3. Drifter tracks for the 8-month period of the study (May 7, 2010 to Dec 31, 2010). The 6 km interpolation grid for the HFR data is shown in gray. The DWH location is shown by the black star.

2.3. NCOM model output

In the present study we used two data-constrained solutions of the NCOM model (Martin, 2000; Barron et al., 2006; Martin et al., 2008). The employed version of NCOM uses a combined σ–z vertical grid with 32 levels and the Arakawa C-grid in the horizontal at 3 km resolution. The data assimilation scheme (Cummings, 2005) currently uses a 3d-variational method, which allows us to assimilate satellite observations of sea surface height and temperature and *in situ* temperature and salinity data from various sources.

The first set of data used in our experiments is the combined set of 3dVar NCOM analyses (computed daily at 0 UTC) and 6-h forecasts (at 6, 12 and 18 UTC) generated by integrating the model from the analysis times. The hourly velocity components were obtained by linearly interpolating these four model outputs within the 24-h window. Since the 6 km HFR interpolation grid (Fig. 3) was configured to coincide with every other node of the NCOM grid, the output currents used for Lagrangian tracking were obtained by picking every other grid point value from the original model grid. These data cover the whole period from May 7 to December 31, 2010. They will be further abbreviated by rNCOM (regional NCOM).

The second set of velocity fields is the ensemble mean of the NCOM runs constrained by the above described data using the ensemble transfer (ET) technique (Bishop and Toth, 1999). The ensemble contained 32 members, generated by perturbing atmospheric forcing derived from the Navy atmospheric model using the time-deformation technique (Wei et al., 2013). Additionally, both vertical and horizontal mixing parameters were perturbed to represent model uncertainties from NCOM sub-grid parameterizations. The mixing parameter perturbations were Gaussian with the means of 0.125, 17.5 and variances of 0.01875 and 0.625 for the Smagorinsky and Mellor–Yamada coefficients respectively. More details on the ET implementation with NCOM can be found in Wei et al. (2013). The set of the ensemble analyses/forecasts (denoted eNCOM further below) was available on the same space-time grid as rNCOM, but for the shorter period of time from May 7 to July 25, 2010. Similar technique was used to project the eNCOM near-surface velocities on the HFR interpolation grid. Hourly velocities in both model outputs were taken from three different vertical levels: 0 m, 2.5 m and 7.5 m.

3. Methodology

3.1. Processing HFR data

Since HFRs measure projections of the surface velocity vectors on the directions $\boldsymbol{r}$ of the radar beams, an algorithm is needed to reconstruct the velocity field from such observations. In the present study we use a combination of the statistical gap-filling technique with the 2dVar interpolation algorithm (Yaremchuk and Sentchev, 2011) for this purpose. The approach is especially suitable for gappy data (Fig. 2) with inhomogeneously distributed observation points and allows to directly control divergence and vorticity of the interpolated field $\boldsymbol{u}$.

The optimal estimate of $\boldsymbol{u}$ is determined by maximizing its likelihood expressed in terms of the Gaussian probability density function $\mathcal{P}(\boldsymbol{u})\sim\exp[-J(\boldsymbol{u})]$. The argument of the exponent (the cost function) is quadratic in $\boldsymbol{u}$ and consists of two terms: $J=J_d+J_r$.

The first term J_d measures the distance between the radial velocity u_k^* observed at the kth point and the corresponding components of the interpolated field $\boldsymbol{u}$ at the observation points:

$$J_d=\frac{1}{2}\left[\sum_{k=1}^{K}\sigma_k^{-2}[(\boldsymbol{u}\cdot\boldsymbol{r}_k)-u_k^*]^2\right] \quad (1)$$

Because of Gaussianity the distance is quadratic in $\boldsymbol{u}$ and scaled at the observation points by the corresponding measurement error variances σ_k^2. The regularization term J_r is introduced to penalize higher spatial derivatives of $\boldsymbol{u}$:

$$J_r=\frac{K}{2A}\int_\Omega[W_u(\Delta\boldsymbol{u})^2+W_d(\Delta\ \mathrm{div}\ \boldsymbol{u})^2+W_c(\Delta\ \mathrm{curl}\ \boldsymbol{u})^2]\,dx\,dy \quad (2)$$

where $\mathrm{div}\,\boldsymbol{u}=\partial_x u+\partial_y v$, $\mathrm{curl}\,\boldsymbol{u}=\partial_x v-\partial_y u$ are the divergence and vorticity respectively, $\Delta=\partial_{xx}+\partial_{yy}$ is the Laplacian operator and A is the area of interpolation domain shown in Fig. 3. The differential operators were approximated by central finite differences on the regular interpolation grid with a step $\delta x=6$ km equal to the radial resolution l_r of the HFR data.

The weights W_u, W_d and W_c have the meaning of the inverse error variances of the corresponding fields and allow to control their magnitude in the interpolation pattern. In the experiments described in the next section, the cost function weights were derived from HFR data statistics and then fine-tuned to maximize the predictability of the drifter trajectories.

Another important aspect of the HFR data processing is gap-filling. The back-scattered HFR signals suffer from distortions of artificial and natural origin, such as atmospheric conditions, sea surface roughness, sea traffic and malfunctions in radar operation. As a consequence, estimates of the radial velocities extracted from the Doppler shifts of the HFR signals become unusable, resulting in numerous gaps in spatial coverage, which was the case with the data we used (Fig. 2). As it is seen from Figs. 1 and 2, most of the gaps have relatively short life time and are more frequent at long ranges. At times, a large amount of data is lost due to improper operation of a single radar when the radial velocities are still observed at nearby locations by the two remaining HFRs.

In this case the gap-filling technique based on the EOF decomposition of the sample covariance matrix (e.g., Beckers and Rixen, 2003) is quite efficient. In the present study we employed a similar method adapted for HFR observations by Yaremchuk and Sentchev (2011). The method usually works well for the observation locations where gaps occupy less than ξ~20–30% of the total observation time. In our case this condition for the gap concentration parameter ξ was satisfied for approximately 60% of the points where radial velocities were observed.

The gap-filling procedure was performed in several steps. First, a set of cross-validation (CV) points randomly distributed across the 8-month observation period was removed from the data. On the average, 1% of the data were set aside from each hourly observation of the radial velocities. Second, iterative processes of estimating the covariance matrix and the gap-filling were performed for different numbers M of the gap-filling EOFs. Third, the optimal value of M was selected by minimizing the gap-filling error e_g which was assessed using the temporarily removed observations in the CV points. Finally, the CV points were added to the data set and the remaining gaps were filled using the optimal number of EOFs.

It is noteworthy that the optimal value of M allows for separation of signal from noise in the data space (e.g., Yaremchuk and Sentchev, 2011): spatial structures, described by M EOFs with largest amplitudes can be attributed to the "resolved signal" whereas variability described by the rest of the EOFs can be treated as noise. In our experiments the optimal value of M varied in the range between 25 and 64, accounting for 60–80% variability of the radial velocities. The noise covariance matrix C had negligible correlations between the radial velocity errors, so we used the inverse diagonal elements of C for weighting the misfits between the observed and interpolated radial velocities (Eq. (1)).

In the course of numerical experiments the gap-filling was performed in three sets of points characterized by three values of $\xi = 50, 30$ and 15%. The filled points contributed respectively by 28, 9 and 1.3% to the total number (6 324 530) of the observed radial velocities. After normalization by the rms variance of the observed radial velocities the gap-filling errors varied between 0.56 and 0.64 for the different values of ξ.

3.2. Computing trajectories and their predictability

Drifter tracks were used to evaluate errors of the particle trajectories corresponding to the velocity fields $\boldsymbol{u}$ that were obtained either from HFR observations or from the model. Each drifter trajectory was divided into 4.5-day segments and the actual drifter positions at the beginning of the segments were taken as the initial condition for the virtual particle release. 1000 particles were released within each segment into the 2d velocity field described by

$$\frac{d\boldsymbol{x}}{dt} = \boldsymbol{u}(\boldsymbol{x}, t) + \boldsymbol{u}'(\boldsymbol{x}, t) \tag{3}$$

where $\boldsymbol{x}$ is the position of the particle and $\boldsymbol{u}'$ is the stochastic contribution of the sub-grid scale variability and the measurement uncertainty. The model used to determine $\boldsymbol{u}'$ is a random walk model

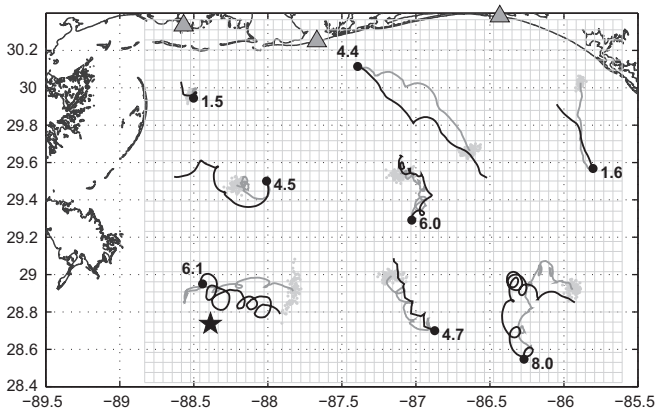

Fig. 4. Examples of the mean virtual drifter trajectories (gray) used for assessing the LP skill and the corresponding real drifter tracks (black). The clouds of light gray dots demonstrate the spread of the virtual trajectories around the mean at the end point. Launch points of the virtual drifters are shown by black circles. Numbers show the integration time in days.

(e.g., Ullman et al., 2006) with the effective diffusion coefficient of 1.5×10^6 cm^2/s, a typical value of the Smagorinsky diffusion coefficient from the NCOM model. This approach provides a consistent Lagrangian tracking techniques for the velocity fields obtained from both HFR observations and the assimilative models (Fig. 4).

The prediction of the particle trajectory was done by integrating Eq. (3) with a fourth-order Runge–Kutta scheme. At hourly times τ of each integration of (3), the prediction error e_τ was computed as the distance between the location $\boldsymbol{x}_c$ of the centroid of the particle cluster and the actual drifter position $\boldsymbol{x}_d$: $e_\tau = |\boldsymbol{x}_c(\tau) - \boldsymbol{x}_d(\tau)|$. Prediction errors were then averaged $\langle\rangle$ over all the available segments, whose number n varied between 71 ($\tau = 1$ h) and 20 ($\tau = 9$ days). Since the segment length (4.5 days) was chosen as the mean decorrelation time scale of the HFR-derived (4.3 days) and model (4.7 days) velocity fields, prediction error estimates for each segment were assumed to be statistically independent. Error bars for $\langle e \rangle$ were computed as the 70% confidence intervals derived from the χ^2 distributions with $2n$ degrees of freedom.

In addition to the virtual particle trajectories, the mean separation $\langle|\boldsymbol{x}_d(\tau) - \boldsymbol{x}_d(0)|\rangle$ between the actual drifter position at time τ and its initial position $\boldsymbol{x}_d(0)$ at the segment was also computed. The prediction skill γ was defined by

$$\gamma_\tau = \frac{\langle e_\tau \rangle}{\langle|\boldsymbol{x}_d(\tau) - \boldsymbol{x}_d(0)|\rangle} \tag{4}$$

Thus, the skill was estimated relative to the "position persistence scenario" which represents a search based on the last known position $\boldsymbol{x}_d(0)$ in the complete absence of information on the surface currents.

4. Results

Computations reported in this section had two objectives. The first one was to explore how preprocessing of the HFR data affects the LP skill of the reconstructed velocity fields. The second one was to compare in terms of the LP skill the HFR-derived velocities with the available operational data-assimilation products, unconstrained by the surface velocity data.

4.1. Prediction skill of the HFR-derived currents

4.1.1. Impact of the prior statistical assumptions

As it has been mentioned in Section 3.1, result of 2dVar interpolation crucially depends on the statistics of the interpolated

fields, which is expressed in terms of the inverse error variances σ^{-2}, W_u, W_d and W_c of the cost function.

The interpolation error variances σ^2 which measure the misfit between the observed radial velocities and their counterparts derived from the interpolated pattern (Eq. (1)) were estimated as the diagonal values of the noise covariance matrix (Section 3.1). Their values varied between 16 cm^2/s^2 in the close proximity from the radars to about 150–250 cm^2/s^2 at far ranges (150–240 km). The regularization weights (Eq. (2)) were first estimated by considering the typical spatial scales of the reconstructed velocity field and then fine-tuned to obtain the best skill in predicting real drifter trajectories.

As a rough estimate of W_u, we assumed that the smallest spatial scale l is twice the range discretization $l \sim 2l_r = 12$ km of the radial velocities. This assumption translates into the estimate $l \sim (\sigma^2/W_u)^{1/4} = 2l_r$, or $W_u \sim \sigma^2 l_r^4/16$. Fine tuning of this weight against the drifter data (with $W_c = W_d = 0$) has shown that the best LP skill is achieved at $W_u = 0.05\sigma^2 l_r^4$, a value, corresponding to the cut-off scale $2.15l_r$. The resulting mean interpolation error $\langle \boldsymbol{e} \rangle = \langle \sqrt{KJ_d} \rangle$ was 0.32, fairly consistent with the estimated noise level in the radial velocity data.

After fixing the optimal value of $\langle \boldsymbol{e} \rangle$, a large set of 2dVar interpolation experiments has been conducted to optimize the values of W_c and W_d. These experiments have shown that $\langle \gamma \rangle$ (the value of γ_τ averaged over the forecast times between 0 and 9 days) is weakly sensitive to W_c and exhibits a slight decrease as the value of W_c approaches zero. For this reason the corresponding term was eliminated from the cost function.

In contrast to W_c, varying W_d which suppresses the roughness and magnitude of the divergence, had a significant impact on the LP skill at the forecast times exceeding 3–4 days (Fig. 5). The optimal value of W_d was found to be 8×10^{-3} cm^4 s^2, and resulted in the 2–3 smaller rms magnitude of the divergence compared to the curl of the surface currents. The better LP skill at larger forecast times can be partly explained by the fact that suppressing the divergence tends to increase the accuracy in reconstructing the geostrophic component of the flow, which is characterized by slower variability than tidal and wave-induced components of the surface currents.

Fig. 5 provides an indication that despite poorer Lagrangian statistics at longer time scales, the effect appears to be statistically significant: the error reduction observed at $\tau > 3$ days persists throughout the entire forecast time interval.

In terms of the absolute value, the LP error grows from 12–20 km at the forecast times of 1–2 days to 35–50 km at $\tau = 5$–9 days. The short-term forecast errors are consistent with the recent LP study of Kohut et al. (2012) who validated HFR-derived currents against six drifters in the region of the Mid-Atlantic Bight and obtained the values of 8–14 km for the forecast times of 1–2 days.

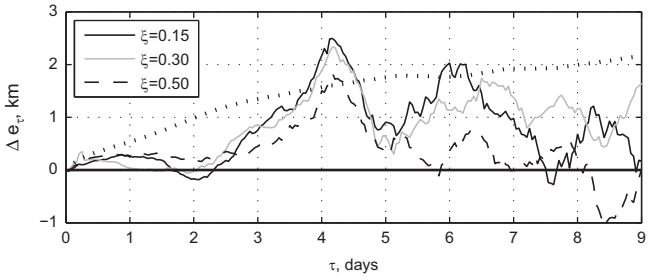

Fig. 5. Difference Δe_τ between the forecast errors of the 2dVar interpolated HFR fields obtained with $W_d = 0$ and $W_d \neq 0$ with various values of the gap concentration parameter ξ. 70% confidence limit for the difference is shown by the thick dotted line. Positive values correspond to smaller forecast error of the divergence-penalizing interpolation ($W_d \neq 0$).

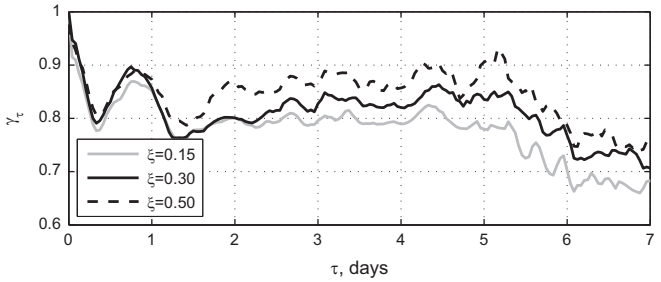

Fig. 6. Drifter forecast skill γ_τ as a function of the forecast time τ for the results of 2dVar interpolation of HFR data with various values of the gap concentration parameter ξ for the case $W_d \neq 0$.

When referenced to the persistence errors (Eq. (4)), these numbers correspond to the values of γ_τ around 0.65–0.7, that is 25–30% better than those shown in Fig. 6. Taking into the account more complex (less deterministic) structure of the flow, poorer quality of the HFR data (Fig. 2) and confinement of most of the drifters to the outer regions of the HFR footprint (Fig. 1), the LP skill of the 2dVar algorithm can be considered as satisfactory.

4.1.2. *Impact of the gap-filling*

Fig. 6 shows that the forecast skill gradually degrades with the decrease of the parameter ξ which defines the upper limit of the gap percentage for filling an observation point with a value derived from statistical analysis.

Because of the extremely intermittent time coverage (Fig. 2) only 1.5% of the observation points were characterized by less than 15% of gaps ($\xi < 0.15$) and all of these points were located at relatively short (20–50 km) distances from the radars, whereas most (75%) of the drifter positions were observed at far ranges (120–180 km) where the gap concentration was fairly high ($\xi \sim 0.4$–0.7) and the accuracy of HFR observations is low.

Table 1 shows improvement (%) of the key parameters of the velocity field normalized by their values obtained without preliminary gap-filling. Apart from the forecast-time-averaged values of γ_τ and e_τ we computed the trace of the correlation matrix C and the relative error e_r between the HFR-derived velocities $\boldsymbol{u}_r$ and the Eulerian velocity estimates $\boldsymbol{v}_d$ obtained from finite differentiation of the drifter positions in time:

$$\mathrm{trC} = c(u_r, u_d) + c(v_r, v_d); \quad e_r = \frac{1}{2}\frac{\overline{(u_r - u_d)^2 + (v_r - v_d)^2}}{\overline{u_d^2 + v_d^2}}$$

Here c stands for the correlation coefficient and overline denotes averaging over all of the 7117 Eulerian velocities estimated from 297 drifter-days of observations. Zonal u_d and meridional v_d drifter velocity components were assessed every hour using central differences.

As it is seen from the Table, persistent improvement is observed only for the case of $\xi = 0.15$, and its magnitude (1.2–1.6%) approximately corresponds to the relative increase in the number of the radial velocities subject to interpolation (1.3%) after the gap-filling. With the increase of ξ, the number of additional (gap-filled) observations grows dramatically, but they do not result in further improvement of the parameters. Instead, the gap-filling "observations" tend to decrease the proximity between the HFR-derived velocity fields and drifter velocities.

This can be explained by the above mentioned mismatch between the spatial distribution of the drifter trajectories and the density if HFR observations. With a more homogeneous temporal HFR and spatial drifter coverages than shown in Figs. 2 and 3 one may expect better performance of the gap-

Table 1
Changes in the error e_r, correlation tr(C), and the mean LP skills $\langle\gamma\rangle$, $\langle e\rangle$ averaged over the forecast times after the gap-filling performed with various threshold gap concentrations ξ. Numbers (%) are normalized by the results obtained for the velocity fields retrieved by the 2dVar without preliminary gap-filling. Positive values denote improvement (decrease of $e_r, \langle e_\tau\rangle, \langle\gamma_\tau\rangle$ and increase of tr(C).

W_d	ξ	ξ_p	e_r	tr(C)	$\langle\gamma_\tau\rangle$	$\langle e_\tau\rangle$
0	0.15	1.3	0.6	0.4	1.2	1.9
	0.30	9.1	0.2	3.2	−4.2	−2.8
	0.50	28.7	−2.4	−1.1	−7.8	−7.6
8	0.15	1.3	1.1	0.8	1.3	2.0
	0.30	9.1	0.3	1.6	−3.7	−1.9
	0.50	28.7	−2.5	3.7	−5.7	−4.8

filling technique, possibly up to the values of ξ~0.3. This requires additional experimentation with the appropriate data sets.

4.2. Comparison with the NCOM output

Parameters listed in Table 1 were also computed for the available surface and subsurface (0, 2 and 7.5 m) velocity fields of the two NCOM data assimilation runs described in Section 2.3. The 2 m velocities demonstrated the best values of the parameters. However, the HFR-derived velocity fields were still 25–40% better both in terms of the LP (Fig. 7) and discrepancies between the Eulerian velocities.

The NCOM LP error curves in Fig. 7 compare quite favorably with the results of Price et al. (2006) who validated a combination of surface velocities from the ORSA model (Smith et al., 1982) and ECMWF wind-induced currents in the period of 1997–1999 in approximately the same region. The diagnosed average discrepancies were found to be 78 km ($\tau = 3$ days), 229 km ($\tau = 10$ days) and 400–500 km ($\tau = 20$–30 days). It should be noted, however, that the domain considered by Price et al. (2006) extended farther offshore and included regions dominated by mesoscale eddies and currents of the open Gulf.

Compared to the HFR-derived velocities, velocity error e_r for the NCOM fields was approximately 10–15% larger, and the correlation coefficient was smaller by 30%.

In general, both data-driven solutions in Fig. 7 demonstrate similar skills, except for the forecast times exceeding 7 days, where the ensemble solution shows 15–20 km larger discrepancy with the drifters. This could be partly attributed to somewhat poorer statistics of eNCOM, which was available only in the May–June 2010 compared to the full 8-month averaging period of rNCOM.

A substantially better LP skill of the HFR-derived currents is not surprising, because the considered models are not constrained by surface velocity data and also do not account for processes affecting the transport by near-surface currents such as Stokes drift and small-scale turbulent wind–wave interactions. Similarly, the NCOM model has a limited skill in accurate simulation of the spatial structure of tidal and inertial oscillations which have profound signatures in the considered region, and sometimes dominate geostrophic and wind-driven components of the surface flow. In this sense the considered coastal region appears to be more challenging from the LP viewpoint, as it is often dominated by smaller-scale processes neither well resolved by the model nor manifested in the wind forcing. As a result, model-generated trajectories have little or no correlation with the drifter trajectories. In fact, the typical values of the LP skill γ for both NCOM runs were close to unity, sometimes reaching 1.3–1.5 (cf. Fig. 6) meaning that the models, on the average, do not have any LP skill compared to the null assumption of zero surface velocity. This result underlines the potential benefits of assimilating HFR observations into the numerical models of coastal regions.

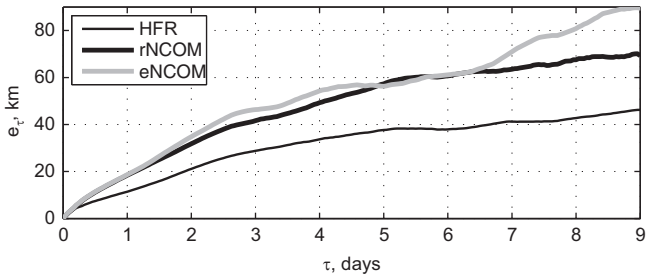

Fig. 7. Drifter forecast error e_τ for the results of 2dVar interpolation of HFR data with enforced smoothness in the divergence field (black curve) and for the NCOM model solutions shown by thick lines.

5. Discussion and conclusions

A set of 37 drifter trajectories was used to evaluate the Lagrangian predictability in the Deep Water Horizon (DWH) oil spill region based on local HF radar data and two data-assimilating regional model runs. The LP was used as a criterion to search for the best parameters of the 2dVar algorithm retrieving the surface velocity fields from the radial velocities recorded by the HF radars.

It is shown that penalizing the magnitude and enforcing smoothness of the divergence field tends to increase LP by 2–6% at the forecast times of 3–9 days while preserving it at the smaller forecast times. Applying preliminary gap-filling technique based on the analysis of spatial correlations of the radial velocities adds an extra 1–2% to the LP and improves correlations between the HFR-derived velocities and the respective Eulerian velocities derived from drifters.

The analyzed drifter set was not conforming with the HFR coverage pattern as most of the drifters were released in the DWH region which is located at the far ranges (150–200 km) off the radar sites. This partially explains a relatively moderate improvement in the LP caused by gap-filling of the observation points covered more than 85% of the time and failure to obtain an improvement if much more numerous observation points with gap concentrations less than 30–50% were taken into account. We also assume that the divergence-related improvement of the LP at the forecast times of 3–9 days could be more visible with a more homogeneous coverage of the domain by drifter trajectories.

Comparing the LP skills of the HFR-derived velocities with surface currents taken from the data-constrained NCOM solutions have shown 25–40% better performance of the observational product. The result is not surprising if previous model/drifter diagnostic studies (e.g., Price et al., 2006; Barron et al., 2007) are compared with validations of the HFR-derived velocities against drifters (e.g., Ullman et al., 2006; Huntley et al., 2011; Kohut et al., 2012). We assume that such a large gap in performance is due to the fact that most of the tested models use relatively simple description of the processes responsible for transport in the top 2 m of the water column, which is strongly affected by the waves/swell and other upper-layer processes controlled by the momentum transfer from the atmosphere. In that respect, assimilation of the HFR data into numerical models is the most straightforward way to improve the situation. Unfortunately, to the best of our knowledge, there has been no assessment of the HFR data impact on the LP skill in the known assimilation studies involving radar observations (e.g., Paduan and Shulman, 2004; Hoteit et al., 2009; Barth et al., 2010; Yu et al., 2012).

Comparison of the model runs driven by different data assimilation algorithms has shown virtually no difference between the ET and 3dVar methods. We attribute the departure of the eNCOM curve from rNCOM at $\tau > 7$ d in Fig. 7 to relatively poor statistics of the 2.5 month eNCOM period characterized by an average duration of a drifter trajectory of 16 days. Given this limitation, the result

still appears to be inconsistent with the conclusions of Scott et al. (2012) who have shown that using a multi-model ensemble mean provides a significant (20%) improvement of the LP in the Equatorial Atlantic. The inconsistency could be caused by several reasons, such as better statistics (~3000 vs 297 drifter-days), negligible tides and much coarser (20–30 km vs 3 km) resolution in the LP computations of Scott et al. (2012). It should be also noted that the LP skill demonstrated by NCOM in the DWH region ($e_1=20$ km, $e_7=67$ km, Fig. 7) is still better than the best ensemble-mean estimates ($e_1=21$ km, $e_7=122$ km) of Scott et al. (2012) in the Equatorial Atlantic.

Our results also show that substantial LP improvements can be achieved by preprocessing HFR data with a combination of the gap-filling technique and 2dVar interpolation tuned to suppress the divergence field. Apart from a much (20–30%) better LP compared to the considered data-driven model runs, interpolated HFR radial velocities are less noisy and continuous in space and time. These properties make them attractive for assimilation into numerical models as the interpolated HFR velocities are less prone to spurious modes generated by the raw radial velocities often characterized by highly intermittent patterns, especially at the outer regions of the HFR footprint. The issue of efficiency of assimilating either raw radial velocities or their projections on the model grid remains an open question, which requires further research.

Acknowledgements

Some of the drifter data were obtained courtesy of Prof. R. H. Weisberg and the USF Ocean Circulation Group, through a coordinated ocean observing and modeling program focusing on the West Florida Shelf. Helpful discussions with Prof. L. Piterbarg are acknowledged. This research was made possible in part by a grant from BP/The Gulf of Mexico Research Initiative through the Consortium for Advanced Research on Transport of Hydrocarbon in the Environment (CARTHE).

References

Barrick, D., Fernandez, V., Ferrer, M., Whelan, C., Breivik, C., 2012. A short-term predictive system for fro surface currents from a rapidly developed HF radar network. Ocean Dyn. 62, 725–740.

Barron, C.N., Kara, A.B., Martin, P.J., Rhodes, R.C., Smedstad, L.F., 2006. Formulation, implementation and examination of vertical coordinate choices in the Global Navy Coastal Ocean Model (NCOM). Ocean Model. 11, 347–375.

Barron, C.N., Smedstad, L.F., Dastugue, J.M., Smedstad, O.M., 2007. Evaluation of ocean models using observed and simulated drifter trajectories: impact of sea surface height on synthetic profiles for data assimilation. J. Geophys. Res. 112, C7, C07019.

Barth, A., Alvera-Azcrate, A., Gurgel, K.-W., Staneva, J., Port, A., Beckers, J.-M., Stanev, E.V., 2010. Ensemble perturbation smoother for optimizing tidal boundary conditions by assimilation of high-frequency radar surface currents—application to the German Bight. Ocean Sci. 6 (1), 161–178, http://dx.doi.org/10.5194/os-6-161-2010.

Beckers, J.M., Rixen, M., 2003. EOF calculations and data filling from incomplete oceanographic observations. J. Atmos. Oceanic Tech. 20 (12), 1839–1856.

Bishop, C.H., Toth, Z., 1999. Ensemble transformation and adaptive observations. J. Atmos. Sci. 56, 1748–1765.

Cummings, J.A., 2005. Operational multivariate ocean data assimilation. Q. J. R. Meteorol. Soc. 131, 3,583–3,604.

Harlan, J., Terrill, E., Hazard, L., Keen, C., Barrick, D., Whelan, C., Howden, S., Kohut, J., 2010. The integrated ocean observing system High-Frequency radar network: status and local, regional, and national applications. Mar. Tech. Soc. J. 4 (6), 122–132.

Hoteit, I., Cornuelle, B., Kim, S.Y., Forget, G., Kohl, A., Terrill, E., 2009. Assessing 4D-VAR for dynamical mapping of coastal high-frequency radar in San Diego. Dyn. Atmos. Oceans 48, 175–197.

Huntley, H.S., Lipphardt, B.L., Kirwan, A.D., 2011. Lagrangian predictability assessed in the East China Sea. Ocean Model. 36, 163–178.

Kaplan, D., Lekien, F., 2007. Spatial interpolation of surface current data based on open-boundary model analysis. J. Geophys. Res. 112, C12007.

Kohut, J., Roarty, H., randall-Goodwin, E., Glenn, S., Lichtenwalner, S., 2012. Evaluation of two algorithms for a network of coastal HF radars in the Mid-Atlantic Bight. Ocean Dyn. 62, 953–968.

Liu, Y., Weisberg, R.H., Hu, C., Zheng, L., 2011. Trajectory forecast as a rapid response to the Deepwater Horizon oil spill. In: Liu, Y., et al. (Eds.), Monitoring and Modeling the Deepwater Horizon Oil Spill A Record-Breaking Enterprise Geophysical Monograph Series, AGU, Washington, D.C.

Lumpkin, R., Elipot, S., 2010. Surface drifter pair spreading in the North Atlantic. J. Geophys. Res 115, C12017.

Martin, P.J., 2000. A description of the Navy Coastal Ocean Model version 1.0 NRL Rep. NRL/FR/7322-00-9962, 42 pp. Navigation Research Laboratory at Stennis Space Center, MS.

Martin, P., Barron, C., Smedstad, L., Wallcraft, A., Rhodes, R., Campbell, T., Rowley, C., 2008. Software Design Description for the Navy Coastal Ocean Model (NCOM) Ver. 4.0. NRL Rep. NRL/MR/7320-08-9149, 151 pp. Nav. Res. Lab. at Stennis Space Center, MS.

Özgökmen, T.M., Piterbarg, L., Mariano, A.J., Ryan, E.H., 2001. Predictability of drafter trajectories in the tropical pacific ocean. J. Phys. Oceanogr. 31, 2691–2719.

Paduan, J.D., Shulman, I., 2004. HF radar data assimilation in the Monterey Bay area. J. Geophys. Res. 109, C07S09.

Price, J.M., Reed, J., Howard, M.K., Johnson, W.R., Li, Z.G., Marshall, C.F., Guinasso, N.L., Rainey, G.B., 2006. Preliminary assessment of an oil-spill trajectory model using satellite-tracked, oil-spill-simulating drifters. Environ. Model. Softw. 21 (2), 258–270.

Scott, R.B., Ferry, N., Drevillon, M., Barron, C., Jourdain, N., Lellouche, J.-M., Metzger, E.J., Rio, M.-H., Smetstad, O.M., 2012. Estimates of surface drifter trajectories in the equatorial Atlantic: a multi-model ensemble approach. Ocean Dyn. 62, 1091–1109.

Schmidt, R.O., 1986. Multiple emitter location and signal parameter estimation. IEEE Trans. Antenna Propag. AP-34, 276–280.

Shadden, S.C., Lekien, F., Paduan, J.D., Chavez, F.P., Marsden, J.E., 2009. The correlation between surface drifters and coherent structures based on high-frequency radar data in Monterey Bay. Deep-Sea Res. II 56, 161–172.

Smith, R.A., Slack, J.R., Wyant, T., Lanfear, K.J., 1982. The Oil spill Risk Analysis Model of the U.S. Geological Survey. Geological Survey Professional Paper 1227. U.S. Geological Survey, Reston, VA, USA.

Stewart, R.H., Joy, J.W., 1974. HF radio measurements of surface currents. Deep-Sea Res. 21, 1039–1049.

Ullman, D.S., O'Donnell, J., Kohut, J., Fake, T., Allen, A., 2006. Trajectory prediction using HF radar surface currents: Monte Carlo simulations of prediction uncertainties. J. Geophys. Res. 111, C12005.

van Sebille, E., van Leeuwen, P.J., Biastoch, A., Barron, C.N., de Ruijter, W.P.M., 2009. Lagrangian validation of numerical drifter trajectories using drifting buoys: application to the Agulhas system. Ocean Model. 29, 269–276.

Wei, M., Rowley, C., Martin, P., Barron, C., Jacobs, G., 2013. The U.S. Navys RELO Ensemble Prediction System in the Gulf of Mexico. Q. J. R. Meteorol. Soc., in press.

Weisberg, R.H., 2011. Coastal ocean pollution, water quality and ecology: a commentary. MTS J. 45 (2), 35–42.

Yaremchuk, M., Sentchev, A., 2009. Mapping radar-derived surface currents with a variational method. Cont. Shelf Res. 29, 1711–1722.

Yaremchuk, M., Sentchev, A., 2011. A combined EOF/variational approach for mapping radar-derived sea surface currents. Cont. Shelf Res. 31, 758–768.

Yu, P., Kurapov, A.L., Egbert, G.D., Allen, J.S., Kosro, P.M., 2012. Variational assimilation of HF radar surface currents in a coastal ocean model off Oregon. Ocean Model. 37.